ELSEVIER

Journal of Structural Geology 29 (2007) 599–613

JOURNAL OF STRUCTURAL GEOLOGY

www.elsevier.com/locate/jsg

Pseudotachylytes in an ancient accretionary complex and implications for melt lubrication during subduction zone earthquakes

Kohtaro Ujiie [a,*], Haruka Yamaguchi [a], Arito Sakaguchi [a], Shoichi Toh [b]

[a] *Institute for Research on Earth Evolution, Japan Agency for Marine-Earth Science and Technology, 3173-25 Showa-machi, Kanazawa-ku, Yokohama 236-0001, Japan*

[b] *The Research Laboratory for High Voltage Electron Microscopy, Kyushu University, 6-10-1 Hakozaki, Higashi-ku, Fukuoka 812-8581, Japan*

Received 2 June 2006; received in revised form 30 October 2006; accepted 30 October 2006
Available online 22 January 2007

Abstract

Pseudotachylyte-bearing fault zones, found in the Shimanto accretionary complex, southwest Japan, developed during subduction or underplating at seismogenic depths. The pseudotachylytes occur in narrow dark veins less than a few millimeters thick that are sharply bounded by foliated cataclasites that originated from a mélange. The microstructures of pseudotachylytes are represented by a fragment-laden, glass-supported texture resulting from the rapid cooling of the frictional melt. Transmission electron microscopy reveals the presence of glass in which euhedral microcrystals of mullite are locally developed. The compositions of the pseudotachylyte matrix and the characteristics of the unmelted grains and microlites in the matrix suggest that frictional melting occurred in an illite-rich slip zone with a minimum melting temperature of 1100 °C. The viscosities of the frictional melt were calculated from the pseudotachylyte matrix composition as well as from the volume fraction and aspect ratio of the unmelted grains. The viscosities at 1100 °C range from 85 to 290 Pa s, and the corresponding shear resistance along a 1-mm-thick melt layer at a slip rate of 1 m/s was 0.1–0.3 MPa. The formation of a melt layer in an illite-rich slip zone can possibly induce large stress drops, increase the slip rate and enhance rupture propagation, which together could affect the earthquake magnitude in a subduction zone.

Keywords: Pseudotachylyte; Frictional melting; Dynamic weakening; Accretionary complex; Subduction zone

1. Introduction

Approximately 85% of the seismic moment release occurs at subduction zones (Scholz, 2002). Previous studies have revealed that temperature limits of ~100–150 °C and ~350–450 °C coincide with the updip and downdip limits, respectively, of the seismogenic zone in subduction zones (Hyndman et al., 1997; Oleskevich et al., 1999). The updip limit of the seismogenic zone appears to be controlled by diagenetic to low-grade metamorphic processes along subduction thrusts (Moore and Saffer, 2001), whereas the downdip limit may correlate with the onset of plastic deformation (Hyndman et al., 1997). For accretionary margins such as Nankai and Cascadia, the seismogenic zone is located mainly beneath the accretionary prism. In contrast to the shallow subduction thrusts where the Ocean Drilling Program has drilled boreholes (Ujiie et al., 2003), subduction thrusts at seismogenic depths are not yet accessible for study; hence, the mechanisms and dynamic processes of seismic slip in subduction zones are not yet well understood.

An accretionary complex consists mainly of offscraped and underplated rocks (Moore, 1989). Some underplated rocks in ancient accretionary complexes may record deformation related to paleo-subduction thrusts (Fisher and Byrne, 1987; Ujiie, 2002). Thermal and metamorphic analyses suggest that some underplated rocks were subducted in the thermal regime of the seismogenic zone (Vrolijk et al., 1988; Ohmori et al., 1997), so that on-land analogs of subduction thrusts at seismogenic depths may be exposed in underplated rocks of ancient accretionary complexes.

* Corresponding author. Tel.: +81 45 778 5467; fax: +81 45 778 5439.
E-mail address: ujiiek@jamstec.go.jp (K. Ujiie).

0191-8141/$ - see front matter © 2006 Elsevier Ltd. All rights reserved.
doi:10.1016/j.jsg.2006.10.012

Recently, pseudotachylytes (i.e., solidified frictional melts produced during seismic slip) have been discovered in the Shimanto accretionary complex in southwest Japan (Ikesawa et al., 2003) and the Kodiak accretionary complex in Alaska (Rowe et al., 2005). They are considered to have developed in underplated rocks at seismogenic depths and thus may help our understanding of the dynamics of earthquake faulting in subduction zones. Descriptions of pseudotachylytes in accretionary complexes are as yet severely limited: there is little information on their microstructures, compositions, and melting temperatures. At present, it is uncertain how the frictional melting of subducted material affects seismic slip. The high viscosity of a frictional melt may restrain seismic slip (Scholz, 1980), alternatively, the generation of a low-viscosity melt from subducted material may cause an increase in the slip rate and control the efficiency with which stored strain energy is released, thus, increasing the earthquake magnitude in subduction zones. In contrast to pseudotachylytes in other geological settings, such as continental plutonic and metamorphic rocks that indicate fault weakening by friction-induced melts occurs during earthquakes (Spray, 1993; Di Toro et al., 2006), the effects of frictional melting on a seismic slip in a subduction zone remain poorly understood, reflecting the paucity of research on pseudotachylyte generation in subducted material.

In this study, we analyzed pseudotachylytes from the Shimanto accretionary complex of eastern and western Shikoku, southwest Japan (Fig. 1). We first describe the characteristics of the fault rocks and the microstructures and compositions of the pseudotachylytes, and then we calculate the viscosities and cooling times of the frictional melts. Based on these descriptions and calculations, we discuss the role of frictional melting on seismic slip in the paleo-subduction zone. Our results may be applicable to fault zones in other sediment-rich subduction zones, where the subducted material is similar to the material in the coseismic slip zones of the Shimanto accretionary complex.

2. Paleotectonic settings of pseudotachylyte-bearing fault zones

The Shimanto accretionary complex is exposed along the Pacific side of southwest Japan and is divided into Cretaceous and Tertiary units (Fig. 1a). It consists mainly of offscraped coherent turbidites and underplated tectonic mélange, and it represents an ancient analog of the Nankai accretionary margin where earthquakes larger than magnitude (M) 8 are generated repeatedly (Ando, 1975; Taira et al., 1988). Pseudotachylyte-bearing fault zones occur in the Late Cretaceous Shimanto accretionary complex of eastern (Mugi area) and western (Okitsu area) Shikoku.

The paleotectonic settings of the pseudotachylyte-bearing fault zones have been examined by Ikesawa et al. (2003) and Kitamura et al. (2005) and are briefly summarized here. In both the Mugi and Okitsu areas, the pseudotachylyte-bearing fault zones separate offscraped coherent turbidites above from the mélanges below (Fig. 1b and c). The mélanges consist of a sheared black shale matrix with blocks of pillow and massive basalt, hemipelagic red shale, and sandstone. They display the tectonic disruption of ocean floor stratigraphies caused by layer-parallel shear and vertical loading during subduction. These disrupted stratigraphies are imbricated at least five times in the mélanges, delineating a duplex structure (Fig. 1b and c). The possible tectonic settings of these pseudotachylyte-bearing fault zones in the Shimanto accretionary complex are (1) plate boundary subduction thrusts, (2) roof thrusts of duplex structures, (3) out-of-sequence thrusts, and (4) intracrustal faults. The first and second are associated with the processes of subduction and underplating, respectively. In contrast, the third and fourth are related to later exhumation processes.

The foliation of the mélanges and the shear surfaces of the pseudotachylyte-bearing fault zones generally strike east–northeast and dip steeply northward, showing that these fault zones are subparallel to the mélange fabric formed during subduction. This is expected in the subhorizontal subduction thrust and flat parts of the hinterland-dipping duplex structure (i.e., floor and roof thrusts) because the mélange fabric formed during subduction is generally subhorizontal (Fisher and Byrne, 1987; Ujiie, 2002). In contrast, out-of-sequence thrusts and intracrustal faults crosscut the mélange fabric at various angles. The kinematics of the pseudotachylyte-bearing fault zones indicate a southward-directed, sinistral reverse shear sense (Fig. 1b and c), which is consistent with the shear directions of both the mélanges and the underplating-related thrusts, and with the relative plate motion during the Late Cretaceous (Onishi and Kimura, 1995; Kitamura et al., 2005). The thermal structure commonly shows a sharp discontinuity across the out-of-sequence thrusts and the intracrustal faults with a large displacement, resulting in a thermal inversion across the faults (e.g., Sakaguchi, 1996; Ohmori et al., 1997). However, the maximum paleotemperatures determined by vitrinite reflectance indicate that there was no distinct thermal inversion across the pseudotachylyte-bearing fault zones (Ikesawa et al., 2003; Kitamura et al., 2005). Considering the thermal structures in subduction zones (e.g., Underwood et al., 1993), the isotherm is nearly parallel to both the subduction thrust and roof thrust of the hinterland-dipping duplex for at least several kilometers without distinct thermal inversion across these thrust faults. Therefore, the pseudotachylyte-bearing fault zones are interpreted to represent subduction thrusts or the roof thrusts of the duplex structures rather than out-of-sequence thrusts and intracrustal faults (Fig. 2).

The maximum paleotemperatures of the host rocks were in the range of 170–190 °C and 230–270 °C in the Mugi and Okitsu areas, respectively. If we adopt a paleogeothermal gradient of 50 °C/km, as recorded in the Late Cretaceous Shimanto accretionary complex (Sakaguchi, 1996), the corresponding depths are 3.2–4 km and 4–6 km in the Mugi and Okitsu areas, respectively. Thus, we can infer that the pseudotachylyte-bearing fault zones occurred at seismogenic depths in a subduction zone (Marone and Scholz, 1988).

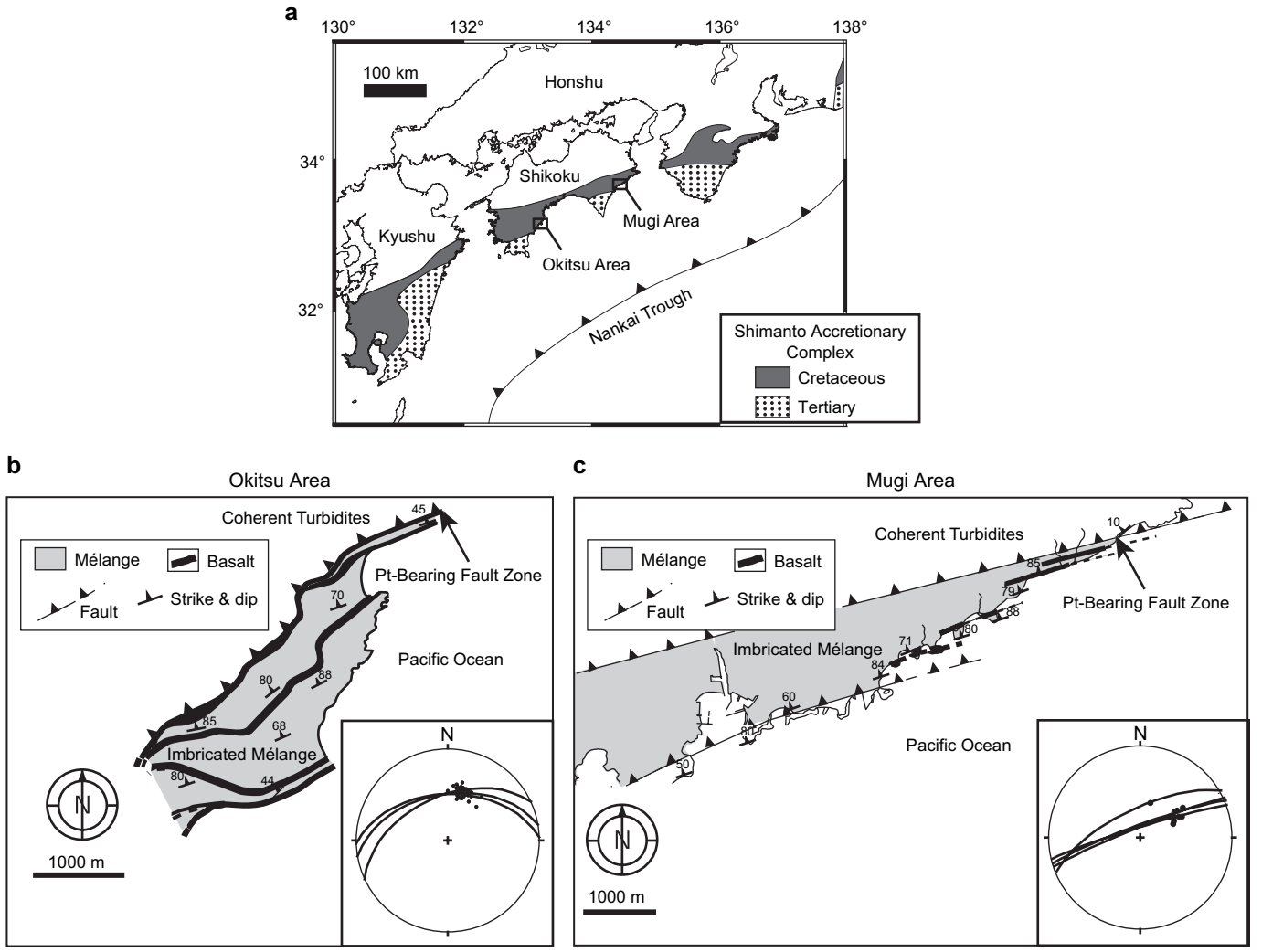

Fig. 1. (a) Distribution of the Shimanto accretionary complex in southwest Japan and locations of the Mugi and Okitsu areas. Geological maps of (b) Okitsu and (c) Mugi areas. Insets show lower hemisphere equal-area projections of shear surfaces (great circles) and slickenlines on shear surfaces (solid dots) in the pseudotachylyte- (pt-) bearing fault zones in the Mugi and Okitsu areas.

3. Characteristics of pseudotachylyte-bearing fault zones

The pseudotachylyte-bearing fault zones in the Mugi and Okitsu areas are ~1–2 m and ~2–5 m thick, respectively. They are composed of foliated cataclasites and dark veins (Fig. 3). In contrast to the mélange fabrics formed mainly by independent particulate flow and pressure solution (Onishi and Kimura, 1995), the pseudotachylyte-bearing fault zones

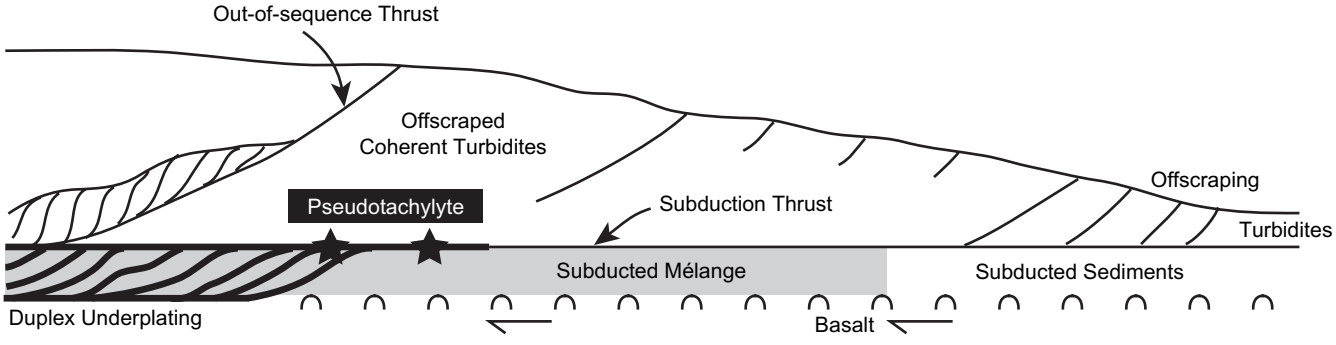

Fig. 2. Paleotectonic settings of the pseudotachylyte-bearing fault zones deduced from geological maps, field observations, kinematics, and thermal data of the Late Cretaceous Shimanto accretionary complex in the Mugi and Okitsu areas. The half arrows indicate the subduction direction. The thick lines indicate cataclastic thrust zones developed at seismogenic depths in the subduction zone.

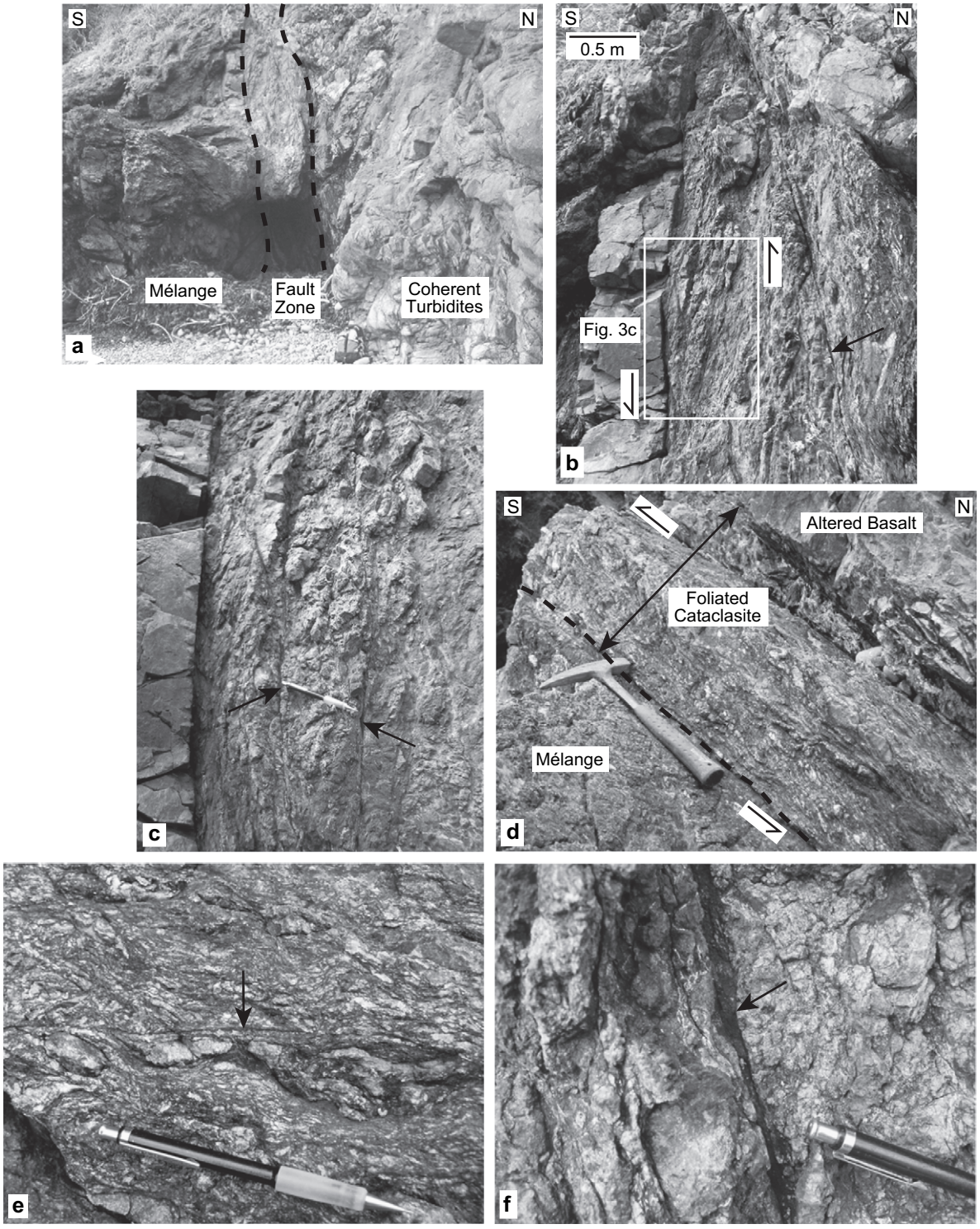

Fig. 3. Characteristics of pseudotachylyte-bearing fault zones in the Mugi (a–c and f) and Okitsu (d and e) areas. (a) A ~1- to 2-m-thick fault zone bounded by coherent turbidites above and mélanges below, showing cataclastic deformation at the top of the mélange. (b) Foliated cataclasite exhibiting asymmetric fabric. The half arrows indicate the shear sense of the foliated cataclasite. The thin, continuous dark vein is indicated by the black arrow. (c) Enlarged view of the foliated cataclasite. The black arrows indicate narrow dark veins less than a few millimeters thick. (d) A fault rock showing the coexistence of altered basalt and foliated cataclasite. The white fragments represent brecciated cement materials of ankerite and quartz. The half arrows indicate the shear sense of the foliated cataclasite. The thick broken line indicates the lower boundary of the fault zone. (e) A dark vein (black arrow) that sharply cuts the foliated cataclasite. The white fragments represent brecciated cement materials of ankerite and quartz. (f) Enlarged view of the dark vein (black arrow).

reflect a greater intensity of brittle deformation at the top of the mélanges.

The foliated cataclasites are defined by the alignment of fragments of sandstone and vein in a shale matrix, which are oriented at less than 30° to the boundaries of the fault zone (Fig. 3b–d). The fragments along the cataclastic foliations commonly exhibit asymmetrical shapes. The mineralogy of the foliated cataclasites in the Mugi area primarily consists of quartz, plagioclase, K-feldspar, illite, chlorite, and laumontite. Except for laumontite, these minerals are also included in the mélange in the Mugi area. The laumontite occurs as fragments along the cataclastic foliations or as a vein-filling mineral. These observations suggest that laumontite cementation occurred only in the pseudotachylyte-bearing fault zone. Laumontite is stable in the temperature range of 130–200 °C (Henley and Ellis, 1983), which is consistent with the maximum paleotemperatures in the host rocks. The other dominant vein-filling mineral is quartz, which is locally brecciated into fragments. In the Okitsu area, fragments of basalt are also embedded in the foliated cataclasites (Fig. 3d). The mineralogy of the foliated cataclasites in the Okitsu area consists primarily of quartz, plagioclase, K-feldspar, illite, chlorite, and ankerite. Ankerite and quartz cementations are present in the foliated cataclasites, however, they are commonly brecciated (Fig. 3d and e). Ankerite cementation is absent in the host rocks.

In both the Mugi and Okitsu areas, the dark veins are thin, commonly less than a few millimeters in thickness. They are either parallel or oblique to the fault zone boundaries and sharply bound the foliated cataclasites (Fig. 3b, c, and e). At the outcrop scale, the veins are continuous and straight, and they rarely contain fragments (Fig. 3f). The pseudotachylytes are found in the dark veins.

4. Microstructures of fault rocks

4.1. Foliated cataclasites and ultracataclasites

The microscopic foliation is defined by the preferred orientation of phyllosilicates within the cataclasite matrix (Fig. 4a). Locally, microscopic shear bands defined by the local reorientation of phyllosilicates transect the matrix foliation at low to moderate angles, with their geometries very similar to the *S*-*C* or *S*-*C*-*C*′ fabric. There is a little evidence for flattened or elongated grains with strain shadows and crystal growth, yet dissolution seams are frequently observed in the foliation. These features indicate that the development of the foliation was associated with the pressure solution as well as the mechanical rotation and alignment of the grains.

Under the optical microscope, the dark veins consist of an ultracataclasite illite-rich matrix which wraps around fragments of quartz, albite, and K-feldspar (<0.5 mm in diameter) (Fig. 4b). The ultracataclasite matrix also includes Ti- (titanite and rutile) and Fe-rich grains (sizes comprised between ~1 mm and 10 mm). Usually, fragments are randomly distributed in the dark matrix (Fig. 4b). A few dark veins have an asymmetric fabric (i.e., similar to the *S*-*C* fabric) that indicates the same sense of shear as the foliated cataclasites. Repeated

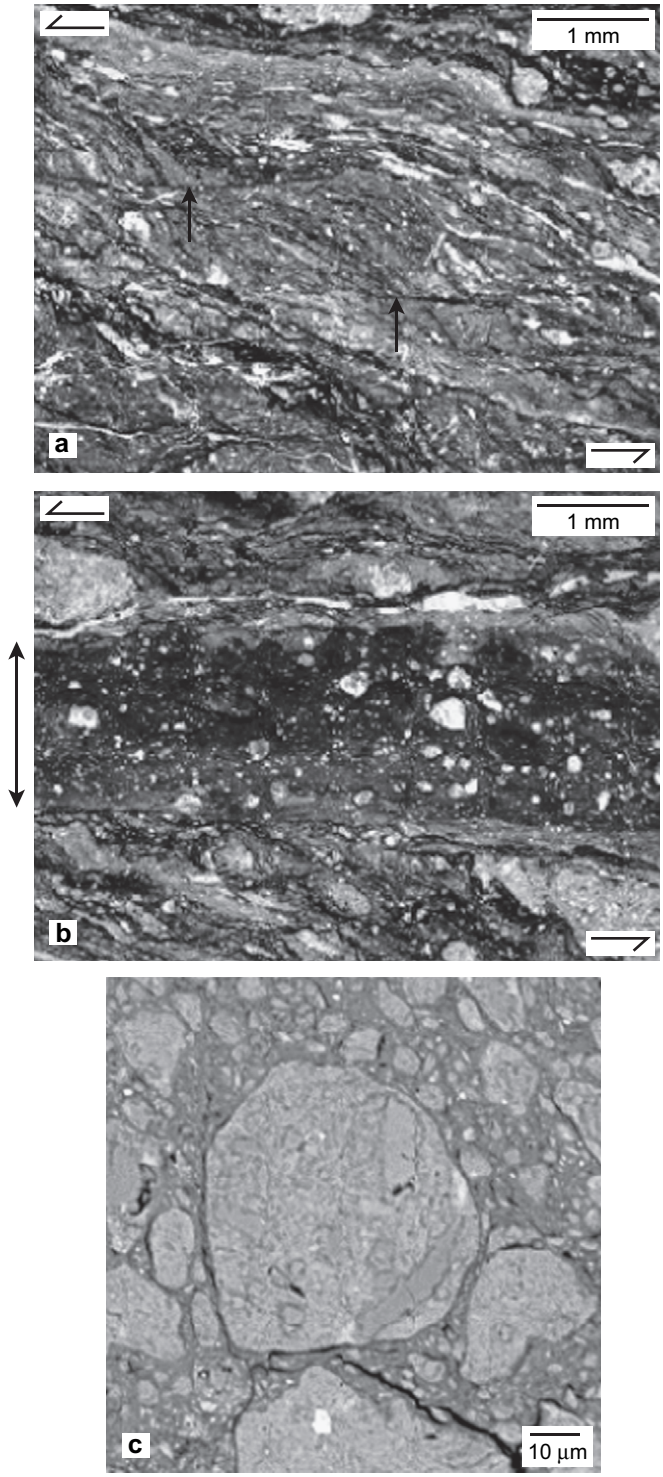

Fig. 4. Microstructures of foliated cataclasites and ultracataclasites. The thin section was cut perpendicular to a dark vein and parallel to a slickenline on the dark vein. (a) The appearance of foliated cataclasites under plane-polarized light. Note that the *S*–like foliation within the cataclasite matrix is locally cut by microscopic shear bands (black arrows). The half arrows indicate the shear sense. (b) The dark veins (double black arrows) at a microscopic scale showing the appearance of ultracataclasite, as seen under plane-polarized light. The foliated cataclasite is sharply cut by the ultracataclasite. The half arrows indicate the shear sense of the foliated cataclasite. (c) Backscattered electron image of the ultracataclasite showing the reworking of the ultracataclasite material. The material comprising the matrices of older (light gray) and younger (gray) ultracataclasites is illite. The very small bright grains are rich in Fe or Ti.

slip events are suggested by the presence of fragments of older ultracataclasites suspended in a matrix of younger ultracataclasite (Fig. 4c). The matrices of both ultracataclasites are made of illite.

4.2. Pseudotachylytes

Some dark veins exhibit the appearance of fault and injection veins, which are typical of pseudotachylytes (Sibson, 1975; Magloughlin and Spray, 1992) (hereafter referred to as fault- and injection-like veins). The boundaries of the fault-like veins are locally embayed (Fig. 5a). Under plane-polarized light, transparent fragments are observed along the fault veins, with sizes ranging from 0.1 to 1 mm (Fig. 5b). The injection-like veins are commonly occupied by transparent material, thinner than 0.5 mm (Fig. 5a). The laumontite/quartz- or ankerite/quartz-type vein is rarely observed along the fault-like vein (Fig. 5a). Enlarged views of the transparent fragments in a fault-like vein are shown in Fig. 5c and d. Subangular to subrounded grains and small dark grains are scattered in the transparent matrix. Under cross-polarized light, the matrix is dark and optically isotropic, and the subangular to subrounded grains are predominantly crystal grains of quartz, K-feldspar, and plagioclase. Crystal grains of illite were not observed in the matrix.

Under the back-scatter electron scanning microscope (BSE-SEM), the homogenous matrix of the transparent material is glassy-like (Fig. 6). Spherical and ellipsoidal vesicles are ubiquitously developed in the matrix. The grains are subangular to subrounded and are predominantly K-feldspar and quartz with minor amounts of albite. Grains of illite are rare in the matrix seen in the BSE images. The volume fraction of the grains is much smaller than that of the matrix (see Section 6). K-feldspar, quartz, and albite commonly exhibit irregular and embayed margins, possibly indicating a marginal melt (Fig. 6). Ti- or Fe-rich bright grains are scattered in the matrix, their sizes ranging from less than 1 μm to more than 10 μm. TiO_2 mineral grains larger than a few micrometers commonly exhibit irregular and embayed margins (Fig. 6d). These microstructures in the BSE images – characterized by vesicles and embayed grains in a homogeneous, glassy-like matrix – are absent in ultracataclasites (e.g., Fig. 4c) and foliated cataclasites.

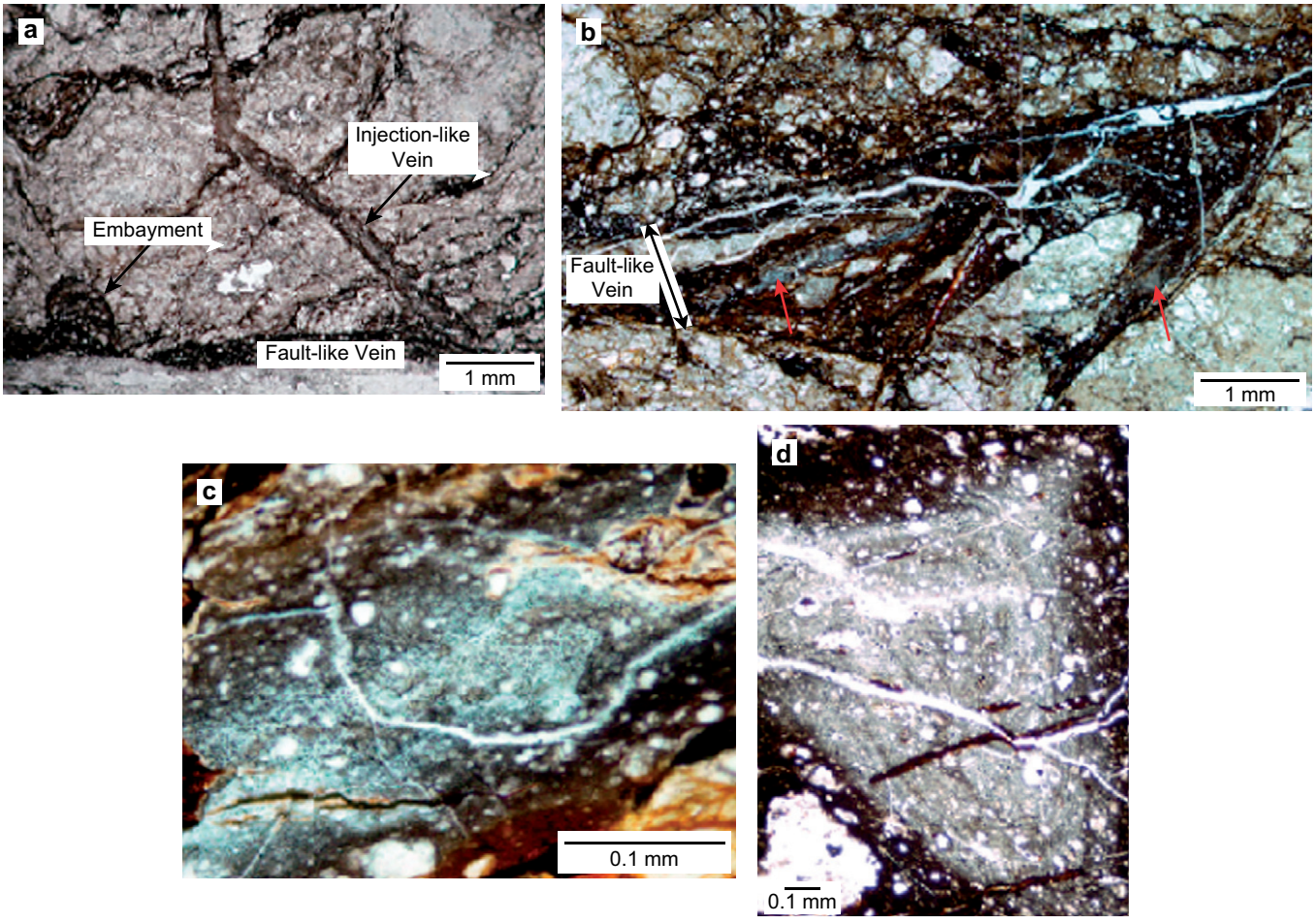

Fig. 5. Transparent material in the fault- and injection-like veins (plane-polarized light). The thin section was cut perpendicular to a dark vein and parallel to a slickenline on the dark vein. (a) and (d) Okitsu area. (b) and (c) Mugi area. (a) Transparent material is preserved in the injection-like vein. Note that the boundary of the fault-like vein is locally embayed and that the thin ankerite/quartz vein (white color at the bottom of the photograph) is developed along the fault-like vein. (b) Transparent fragments (red arrows) in the fault-like vein. (c) and (d) Enlarged views of the transparent fragments showing subangular to subrounded grains and small dark grains scattered in the transparent matrix.

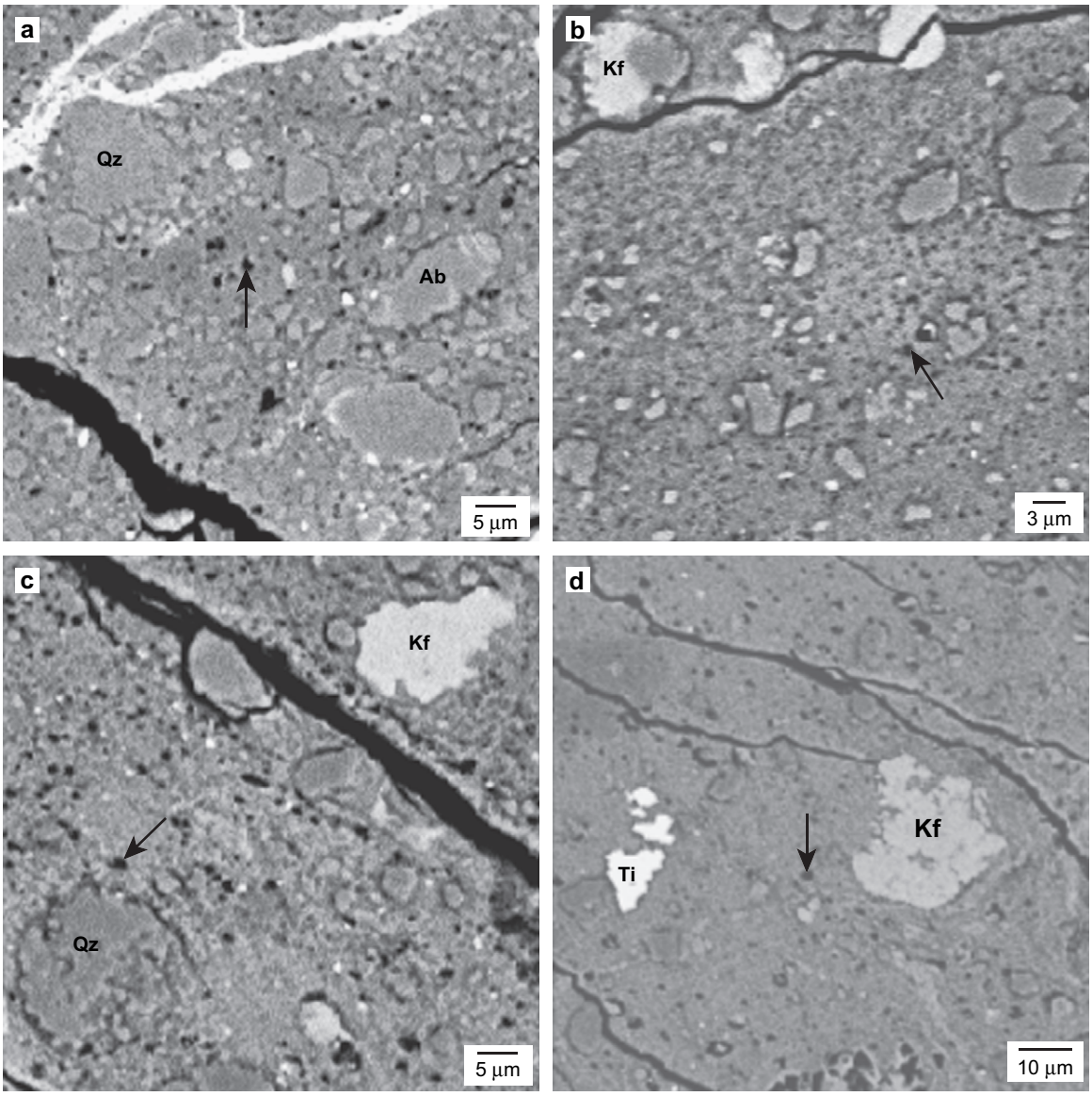

Fig. 6. Backscattered electron images of pseudotachylytes in the Mugi (a and b) and Okitsu (c and d) areas, characterized by vesicles (black arrows), embayed grains, and Ti- or Fe-rich bright grains in the homogeneous matrix. (a) Quartz (Qz) and albite (Ab) grains showing irregular and embayed margins. (b) K-feldspar grain (Kf) showing embayed margins. (c) Irregularly shaped quartz (Qz) and K-feldspar (Kf) grains. (d) K-feldspar (Kf) grains and TiO_2 mineral (Ti) grains of more than a few micrometers in size and exhibiting irregular and embayed margins.

Instead, they are typical of artificial (Spray, 1993) and natural pseudotachylytes (Boullier et al., 2001; Otsuki et al., 2003, 2005), and formed by frictional melting and rapid cooling of the melt.

Transmission electron microscopy (TEM) studies indicate the presence of a glassy matrix. The diffraction pattern of the matrix is characterized by amorphous rings (Fig. 7a). The matrix is observed to be homogeneous in bright-field images, and the diffraction pattern generated from the matrix does not show Bragg spots. In places, euhedral microcrystals are dispersed in the matrix (Fig. 7b). These microcrystals are generally acicular with lengths ranging from 20 to 200 nm. An energy-dispersive spectrometer (EDS) analysis of the euhedral microcrystals detected SiO_2 and Al_2O_3, and the diffraction pattern of the microcrystals is consistent with that of mullite (the Joint Committee on Powder Diffraction Standards-International Center for Diffraction Data, PDF 15-0776). Mullite occurs typically in association with melting of pelitic xenoliths entrained in mafic magma (Thomas, 1922) and can also form when clay minerals are heated to more than 900–1000 °C (Shirozu, 1988). The presence of mullite in the pseudotachylyte matrix was also reported by Otsuki et al. (2003) and Moecher and Brearley (2004). The euhedral microcrystals suspended in the glassy matrix are interpreted as microlites crystallized from the melt during rapid cooling.

Overall, the microstructural features observed in the BSE and TEM images demonstrate that the transparent material found as fragments in the fault-like veins is a pseudotachylyte. Presumably, the fault-like veins initially occurred as pseudotachylyte veins, and the embayed boundaries of the fault-like

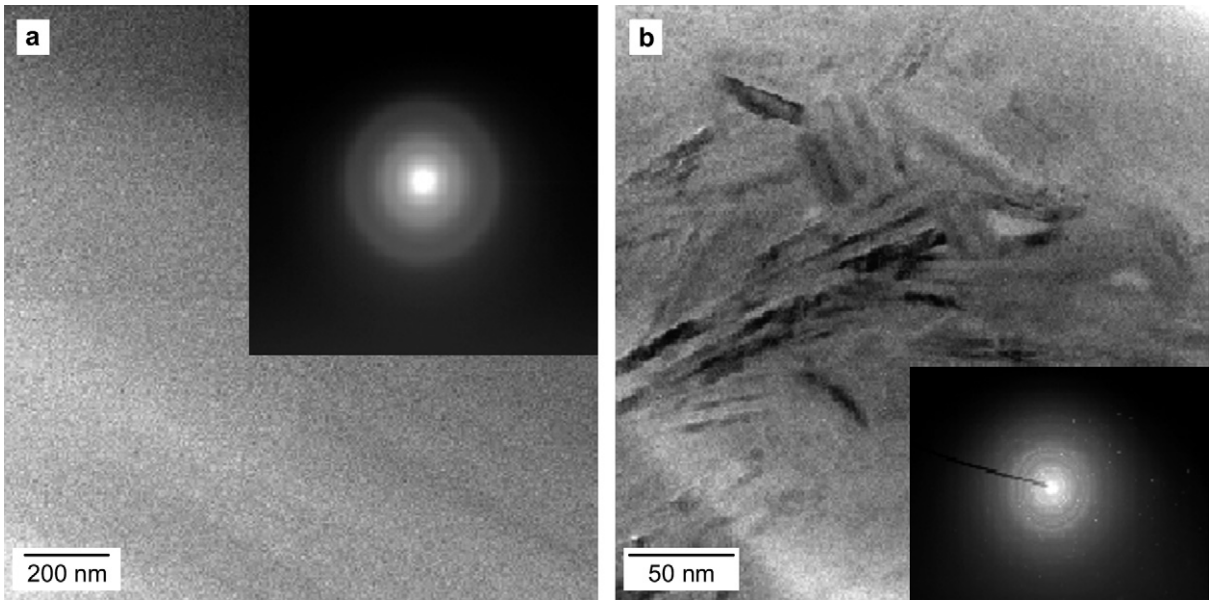

Fig. 7. Transmission electron micrographs of pseudotachylytes (bright-field images). (a) The homogeneous matrix of pseudotachylyte. The upper-right corner shows the amorphous rings in the diffraction pattern. (b) The presence of euhedral microcrystals in the matrix. The lower-right corner shows the diffraction pattern of the microcrystals.

veins could indicate the melting of the wall rocks. The pseudotachylytes were intensely brecciated into fragments, as a result of repeated slip events along the fault-like veins. In contrast, the injection-like veins have survived intense brecciation associated with repeated slip events along the fault-like veins; thus they have been filled by a glassy matrix.

5. Composition of pseudotachylyte matrix and melting temperature

The compositions of the pseudotachylyte matrix and those of illite from the ultracataclasite matrix were determined by an electron probe microanalyzer (JXA–8900RL) installed at the Japan Agency for Marine-Earth Science and Technology, operated at an acceleration voltage of 15 kV with a beam current of 15 nA. Although the volume fraction of the pseudotachylyte matrix is large, minute fragments and vesicles are present in the matrix. To analyze only the pseudotachylyte matrix, we used a focused beam with a diameter of about 1 μm and adopted an average of 5–13 data points as a representative composition. As in the cases of other glassy pseudotachylyte matrices (Spray, 1993; Otsuki et al., 2003), we regarded the missing mass as volatile content. The EDS mainly detected peaks for SiO_2, Al_2O_3, FeO, MgO, and K_2O with or without weak peaks for CaO and Na_2O, so the missing mass was considered to be mostly H_2O. In Table 1, the average compositions of the pseudotachylyte matrix and illite from the ultracataclasite matrix are listed along with the illite composition from Deer et al. (1992). In both the Mugi and Okitsu areas, the composition of the pseudotachylyte matrix is closely comparable with that of illite, and there is no significant spatial compositional variation within the pseudotachylyte matrix.

Because mullite was crystallized during cooling, the presence of mullite in the glassy matrix indicates that frictional melt achieved temperatures higher than 900–1000 °C (Shirozu, 1988; Otsuki et al., 2003). The slip durations of earthquakes are typically a few seconds, and hence, instantaneous melting is expected to occur under disequilibrium conditions (Spray, 1992). K-feldspar, quartz, and albite grains commonly show marginal embayment (Fig. 6), but no distinct change in composition between the grain core and grain margin was visible at the resolution of the electron probe microanalyzer. This suggests that the disequilibrium marginal melting occurred in a closed reaction system separated from the melt matrix and that the breakdown temperatures of the minerals can be used to estimate the melting temperatures (e.g., Otsuki et al., 2003). The breakdown temperatures of albite, K-feldspar, and quartz are 1100, 1150, and 1730 °C, respectively (Spray, 1992). The breakdown temperature of quartz can decrease to 1100 °C in the presence of water (Kennedy et al., 1962). Considering these mineral breakdown temperatures and the presence of mullite microlites in the pseudotachylyte matrix, it is likely that the frictional melts reached a temperature of at least 1100 °C.

6. Viscosity of frictional melt

There are several procedures for calculating the melt viscosity (e.g., Bottinga and Weill, 1972; Shaw, 1972). Assuming an Arrhenian relationship, Shaw (1972) proposed the following empirical formula as a function of melt:

$$\ln \eta = s\left(10^4/T\right) - 1.5s - 6.4, \quad (1)$$

where η is the viscosity, s is the mean slope of viscosity curves on the Arrhenian plots for a given multicomponent mixture, and T is the temperature. This method can predict the melt viscosity simply from the melt composition and is useful for

Table 1
Average composition of pseudotachylyte matrix and illite from ultracataclasite matrix with standard deviations and composition of illite (Deer et al., 1992)

	Mugi area					Okitsu area				Illite (Deer et al., 1992)	
	Ultracataclasaite matrix	Pseudotachylyte matrix				Ultracataclasite matrix	Pseudotachylyte matrix				
		Mg-1	Mg-2	Mg-3	Mg-4		Ok-1	Ok-2	Ok-3		
N	18	11	6	13	5	9	13	8	10		
SiO_2	50.91 ± 0.81	52.55 ± 0.85	51.80 ± 1.50	52.79 ± 0.31	51.65 ± 1.24	49.60 ± 0.86	53.40 ± 0.92	53.05 ± 0.66	52.46 ± 1.13	SiO_2	51.25
TiO_2	1.00 ± 0.68	0.27 ± 0.08	0.16 ± 0.11	0.08 ± 0.01	0.13 ± 0.03	0.19 ± 0.04	0.14 ± 0.07	0.29 ± 0.05	0.21 ± 0.02	TiO_2	0.17
Al_2O_3	27.76 ± 0.91	30.22 ± 0.65	27.88 ± 1.15	27.97 ± 0.00	27.03 ± 0.58	27.28 ± ± 0.41	29.25 ± 0.80	29.03 ± 0.37	28.92 ± 0.36	Al_2O_3	23.53
FeO	4.62 ± 0.94	2.55 ± 0.48	4.68 ± 1.88	3.72 ± 0.12	5.35 ± 0.39	3.89 ± 1.01	2.40 ± 0.49	2.32 ± 0.09	2.28 ± 0.11	Fe_2O_3	2.02
MnO	0.13 ± 0.04	0.21 ± 0.29	0.16 ± 0.04	0.13 ± 0.01	0.19 ± 0.02	0.05 ± 0.02	0.03 ± 0.02	0.05 ± 0.02	0.02 ± 0.01	FeO	0.33
MgO	1.88 ± 0.18	1.63 ± 0.08	1.96 ± 0.29	1.60 ± 0.08	2.15 ± 0.156	2.79 ± 0.31	2.51 ± 0.14	2.52 ± 0.14	2.51 ± 0.05	MnO	–
CaO	1.23 ± 0.61	0.55 ± 0.08	0.66 ± 0.10	0.94 ± 0.49	0.57 ± 0.02	0.57 ± 0.47	0.45 ± 0.40	0.33 ± 0.04	0.42 ± 0.33	MgO	3.32
Na_2O	0.38 ± 0.21	0.13 ± 0.02	0.13 ± 0.01	0.11 ± 0.03	0.15 ± 0.01	0.10 ± 0.02	0.06 ± 0.02	0.06 ± 0.01	0.06 ± 0.01	CaO	0.59
K_2O	7.78 ± 0.40	7.82 ± 0.35	6.92 ± 0.51	6.97 ± 0.08*	6.88 ± 0.14	7.58 ± 0.57	6.90 ± 0.81	8.38 ± 0.52	8.23 ± 0.19	Na_2O	0.05
Total	95.68	95.63	94.34	94.30	94.11	92.04	95.15	96.04	95.12	K_2O	7.61
Missing mass	4.32	4.07	5.66	5.7	5.89	7.96	4.85	3.96	4.88	H_2O^+	5.87
										H_2O^-	5.26
										Total	100.02

N, numbers of analyses.

calculating the temperature dependence of melt viscosity under anhydrous and hydrous conditions. Thus, the viscosities of various types of frictional melts have been estimated from the compositions of pseudotachylyte matrices (Spray, 1993). In this study, we applied Shaw's method to the pseudotachylyte matrices from the Mugi and Okitsu areas using the compositional data listed in Table 1. The calculated results for temperatures between 800 and 1400 °C are shown in Table 2. The matrix viscosities at the minimum melting temperature (1100 °C) range from 21 to 130 Pa s.

The viscosity of a suspension is strongly affected by the volume fraction of solid grains in a suspension (e.g., Lee, 1969; Metzner, 1985); therefore, the matrix viscosity has to be modified to take into consideration the effects of unmelted grains on the suspension viscosity. The relative viscosity (i.e., the ratio of the suspension viscosity to the fluid viscosity) increases exponentially with the volume fraction of the suspended solid grains, and it is affected to a small extent by the aspect ratio of the solid grains. Both effects were accounted for in the following equations by Kitano et al. (1981):

$$\eta_s = \eta_m[1 - (\phi/A)]^{-2} \tag{2}$$

$$A = 0.54 - 0.0125r, \tag{3}$$

where η_m is the matrix viscosity, η_s is the suspension viscosity, and ϕ is the volume fraction of the solid grains. A is a parameter related to the packing geometry of the solid grains, and r is the average aspect ratio of the solid grains. We measured the volume fraction and aspect ratio of the unmelted grains of the seven pseudotachylyte samples using BSE images with a magnification of 1500×. It is possible that the grain size determined from a thin section underestimates its actual size. In this case, the volume fraction of the unmelted grains is higher than that deduced from the BSE images (e.g., Boullier et al., 2001). However, this difference would be very small because the grain size of the unmelted grains is nearly the same in thin sections cut parallel and perpendicular to the shear direction. As shown in Table 3, the volume fraction is small, ranging from 0.09–0.26, and the aspect ratio of the unmelted grains ranges from 1.39–1.58. All samples exhibited a value of 0.52 for parameter A. The same value for this parameter has been reported by Spray (1993) for other pseudotachylyte samples. This value probably reflects the subangular to subrounded shape of the unmelted grains in the pseudotachylytes because the value of A is between that of spheres (0.68) and rough crystals (0.44) (Metzner, 1985). We corrected the matrix viscosities using Eqs. (2) and (3). The suspension viscosities at 1100 °C range from 85 to 290 Pa s (Table 3 and Fig. 8). They are not much higher than those of the matrices at 1100 °C, which primarily reflects the small volume fraction of the unmelted grains.

All the pseudotachylyte samples contain vesicles, which would have increased the viscosity of the melts (e.g., Kraynik, 1988). Taylor (1932) and Shimozuru (1978) proposed the following theoretical equation for the relative viscosity η_r

Table 2
Matrix viscoisities η_m (Pa s)

T (°C)	Mg-1	Mg-2	Mg-3	Mg-4	Ok-1	Ok-2	Ok-3
800	1.6×10^4	2.0×10^3	2.8×10^3	1.4×10^3	7.5×10^3	1.5×10^4	5.1×10^3
900	2.4×10^3	3.7×10^2	5.2×10^2	2.7×10^2	1.3×10^3	2.3×10^3	8.8×10^2
1000	5.0×10^2	93	1.3×10^2	69	2.8×10^2	4.8×10^2	2.0×10^2
1100	1.3×10^2	28	37	21	76	1.3×10^2	57
1200	41	10	13	8	25	40	19
1300	15	4	5	3	9	14	7
1400	6	2	2	2	4	6	3

Mg: sample from the Mugi area; Ok: sample from the Okitsu area.

(the ratio of the viscosity of the fluid, containing a small volume fraction of bubbles, to the viscosity of the fluid):

$$\eta_r = 1 + \phi_b \tag{4}$$

where ϕ_b is the volume fraction of bubbles. Uhira (1980) demonstrated that the experimentally determined relative viscosity agrees with the theoretically predicted viscosity when the volume fraction of bubbles is less than 0.40. Uhira (1980) obtained the following empirical equation:

$$\eta_r = (1 - 1.5\phi_b)^{-0.55} (0 < \phi_b < 0.4). \tag{5}$$

We measured the volume fraction of the vesicles using BSE images with a magnification of 1500×. The size of the vesicles is nearly the same in thin sections cut parallel and perpendicular to the shear direction. The volume fraction of the vesicles ranges from 0.03 to 0.05. Hence, based on the very low volume fraction of the vesicles and on Eqs. (4) and (5), the effect of bubbles on the suspension viscosity was determined to be negligible.

7. Cooling of frictional melt

Neglecting the latent heat of crystallization due to the growth of mullite crystals, the cooling time of frictional melt was calculated from the instantaneous heating of a semi-infinite half-space caused by a sudden increase in the surface temperature, which is expressed as follows (Carslaw and Jaeger, 1959, p. 54):

$$T = \frac{(T_m - T_a)}{2}\left\{\mathrm{erf}\left[(a-x)/2(\kappa t)^{0.5}\right] + \mathrm{erf}\left[(a+x)/2(\kappa t)^{0.5}\right]\right\} \tag{6}$$

where T_m is the melting temperature, T_a is the ambient temperature, a is half the thickness of the melt layer, x is the distance to the center of the melt layer, κ is the thermal diffusivity, and T is the difference between the temperature after time t at a distance x from the center of the melt layer and the ambient temperature at $t = 0$. T_m is defined by the minimum melting temperature recorded in the pseudotachylytes (1100 °C). We used the maximum paleotemperatures in the host rocks as T_a, i.e., 180 °C for the Mugi area and 250 °C for the Okitsu area. The precise thickness of the melt layer remains uncertain because pseudotachylytes are commonly brecciated into fragments with sizes ranging from 0.1 to 1 mm. However, the preservation of pseudotachylytes in the injection-like veins and the presence of the embayed boundaries of the fault-like veins strongly suggest that the melt layer was present along a fault-like vein less than a few millimeters thick and was then disrupted by repeated slip events (Fig. 5). Here, we assume the thickness of the melt layer to be 1 mm ($a = 0.5$ mm), and κ to be 10^{-6} m^2/s (Turcotte and Schubert, 2002).

The calculated cooling history of a 1-mm-thick melt layer is shown in Fig. 9. The result indicates the very rapid cooling of the boundary of the melt layer both in the Mugi and Okitsu areas: T is almost 100 K higher than the host rock temperature after 5 s and close to the ambient temperature after 1 h. Fig. 9 also indicates localized heating along the melt layer. For

Table 3
Grain volume fraction ϕ, grain aspect ratio r, parameter A, and suspension viscosities η_s

	Mg-1	Mg-2	Mg-3	Mg-4	Ok-1	Ok-2	Ok-3
ϕ	0.09	0.26	0.26	0.26	0.13	0.18	0.12
r	1.58	1.56	1.55	1.54	1.39	1.50	1.41
A	0.52	0.52	0.52	0.52	0.52	0.52	0.52
T (°C)	Suspension viscosities η_s (Pa s)						
800	2.3×10^4	7.9×10^3	1.2×10^4	5.4×10^3	1.3×10^4	3.5×10^4	8.6×10^3
900	3.5×10^3	1.5×10^3	2.1×10^3	1.1×10^3	2.2×10^3	5.4×10^3	1.5×10^3
1000	7.3×10^2	3.7×10^2	5.1×10^2	2.7×10^2	4.9×10^2	1.1×10^3	3.4×10^2
1100	1.9×10^2	1.1×10^2	1.5×10^2	85	1.3×10^2	2.9×10^2	97
1200	60	40	53	31	44	92	33
1300	22	16	21	13	17	34	13
1400	9	7	9	6	7	14	5

Mg: sample from the Mugi area; Ok: sample from the Okitsu area.

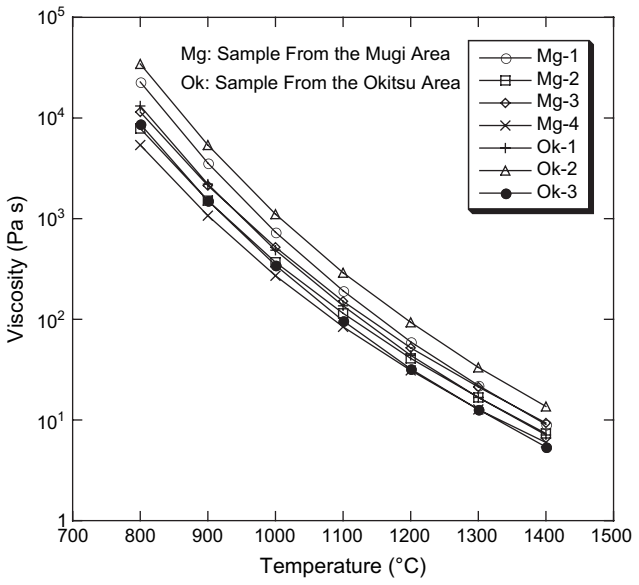

Fig. 8. Suspension viscosity versus temperature for seven samples from the Mugi and Okitsu areas.

example, T never reaches 100 K above the host rock temperature at the point where x is 2.5 mm.

8. Discussion

8.1. Deformation mechanisms of pseudotachylyte-bearing fault zones

The mélange-related deformations occurred pervasively in subducted sediments by layer-parallel shear and vertical flattening, while the main deformation mechanism progressively changed from independent particulate flow to pressure solution (Fisher and Byrne, 1987; Ujiie, 2002). In contrast, the foliation in the pseudotachylyte-bearing fault zones records the mechanical rotation and alignment of phyllosilicates and fragments as well as the development of dissolution seams; the ultracataclasites are considered to reflect frictional wear (Figs. 3 and 4). The paleotectonic settings of the pseudotachylye-bearing fault zones strongly suggest that the cataclastic deformations were not related to exhumation processes (Fig. 2). These features indicate that at seismogenic depths in the subduction zone, pervasive pressure solution creep within the subducted mélange was replaced by cataclasis and pressure solution at the top of the mélange.

The pseudotachylyte-bearing fault zones record cementation, pressure solution, distributed shear, and localized slip, which could occur repeatedly throughout faulting. Laumontite/quartz and ankerite/quartz cementations are observed in the pseudotachylyte-bearing fault zones in the Mugi and Okitsu areas, respectively. The cement material was brecciated during distributed shear, which is represented by cataclastic foliation. The cataclastic foliation and pressure solution seams were locally superposed by shear bands, indicating that the composite planar fabric is consistent with reverse slip displacement (Fig. 4a). Localized slip is represented by dark veins, which sharply cut the cataclastic foliation (Figs. 3 and 4b). The presence of pseudotachylytes and the appearance of fault- and injection-like veins (Fig. 5) indicate that seismic slip accompanying frictional melting occurred in the dark veins. Localized slip along the dark veins was followed by cementation and pressure solution (e.g., Fig. 5a). Fragments of pseudotachylytes and older ultracataclasites suspended in a matrix of younger ultracataclasites represent the reworking of materials due to repeated slip along the dark veins (Figs. 4c and 5b). Accordingly, repeated deformations recorded in the pseudotachylyte-bearing fault zones are interpreted to

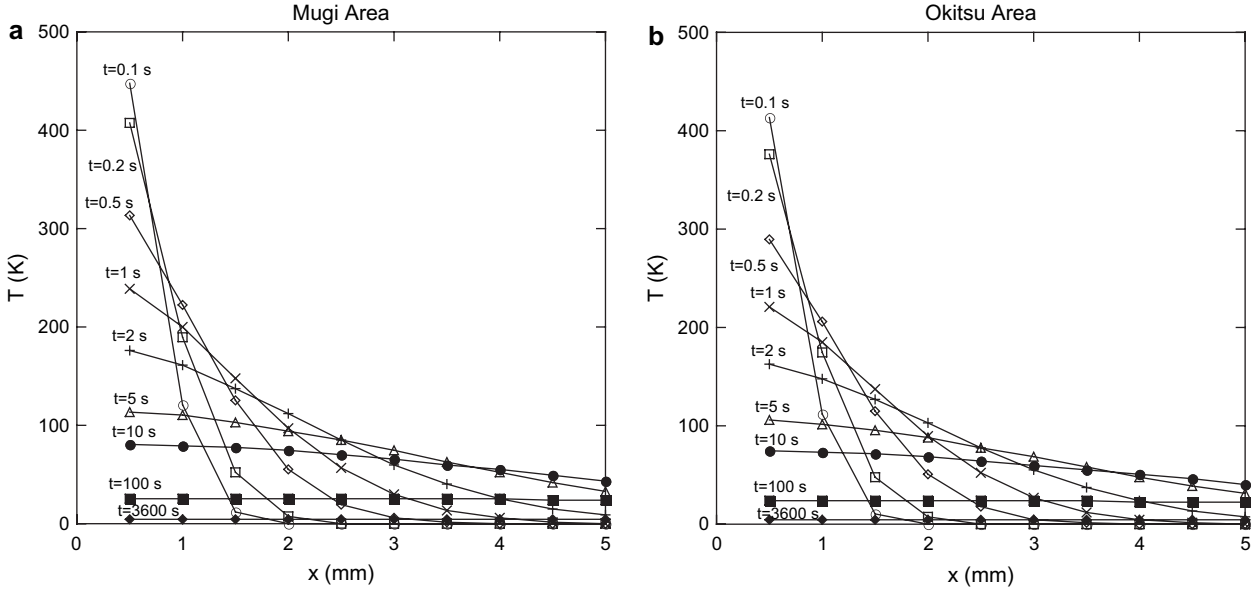

Fig. 9. Cooling history of 1-mm-thick melt layers in the (a) Mugi and (b) Okitsu areas. x is the distance to the center of the melt layer, consequently the limit of that layer is at $x = 0.5$ mm. T is the difference between the temperature of the melt layer and the temperature of the rock before melting.

represent the seismic cycle. In this case, most of the fault displacement would be accommodated by localized slip along the dark veins less than a few millimeters thick.

8.2. Characteristic microstructures and composition of the pseudotachylytes

Small dark grains are scattered in the transparent matrix under plane-polarized light (Fig. 5c and d). A previous study of pseudotachylytes in the Okitsu area (Ikesawa et al., 2003) interpreted the dark grains, which were observed under an optical microscope, as TiO_2 microlites. The BSE images in this study indicate that the very small Ti- or Fe-rich grains scattered in the matrix (Fig. 6) are very similar to spherules, which have been observed in pseudotachylytes elsewhere (Magloughlin and Spray, 1992; Otsuki et al., 2003). However, Ti- or Fe-rich grains are also scattered in ultracataclasites, and the range of their sizes (i.e., less than 1 μm to more than 10 μm) is very similar to that of the pseudotachylytes. Within the pseudotachylytes, TiO_2 grains larger than a few micrometers commonly show irregular and embayed margins (Fig. 6d), and there are no systematic changes in the grain size of the TiO_2 minerals. These features suggest that the Ti- or Fe-rich grains could have existed before frictional melting and that the embayed TiO_2 grains could have resulted from the marginal melting of these preexisting TiO_2 grains.

The presence of injection veins (Fig. 5a) and of embayed grains (Fig. 6) immersed in a glassy homogeneous matrix (Fig. 7) is typical of pseudotachylytes and indicates the rapid cooling of frictional melts (e.g., Boullier et al., 2001; Otsuki et al., 2003, 2005). Mullite microlites suspended in the glassy matrix are also indicative of rapid cooling (Fig. 7b). All these microstructural observations are consistent with the estimated cooling times of $2a \sim 1$ mm thick melt layer to produce the pseudotachylyte vein (Eq. 6 and Fig. 9).

The volume fraction of unmelted grains in the pseudotachylyte matrix varies from 9% to 26% (Table 3), yet the composition of the pseudotachylyte matrix remained nearly constant (Table 1). The marginal melting of albite, K-feldspar, quartz, and TiO_2 minerals was independent of the volume fraction of unmelted grains. The composition of the pseudotachylyte matrix is quite similar to that of illite (Table 1), and illite rarely occurs as unmelted grains in the pseudotachylyte matrix. These features can be explained in terms of the preferential melting of illite because phyllosilicates are consumed to form the melt phase due to their low shear yield strength, fracture toughness, and thermal conductivity as compared to other minerals such as tectosilicates and orthosilicates (Spray, 1992). We suggest that the variations in the volume fraction of the unmelted grains do not reflect differences in the melting degree; instead, they primarily represent the difference in the initial volume fraction of illite in the slip zone before frictional melting.

Previous studies of natural and experimentally generated pseudotachylytes have shown that the pre- or coexistence of ultracataclasite material is a precursor to frictional melting and that the composition of pseudotachylytes is very similar to that of the material comprising the ultracataclasite matrix (e.g., Magloughlin, 1992; Spray, 1995). In the case of the Shimanto pseudotachylytes, illite – the dominant material in the ultracataclasite matrix – would have played an important role in the frictional melting and determination of the composition of the pseudotachylyte matrix. During seismic slip, the frictional melting of illite was likely to be quite pervasive within the preexisting ultracataclasites; the marginal melting of other grains also occurred, but they were probably not thoroughly mixed into the melt, resulting in a matrix composition very similar to that of illite.

8.3. Effects of frictional melting on subduction zone earthquakes

At the minimum melting temperature (1100 °C), the suspension viscosities are low – ranging from 85 to 290 Pa s (Table 3 and Fig. 8). The low viscosities are due to the temperature, H_2O content of illite, and the small volume fraction of unmelted grains. The microstructural observations strongly suggest the past presence of melt layers. The formation of a low-viscosity melt layer would be expected to reduce the shear resistance in the slip zone. Assuming Newtonian behavior of the suspension, the shear resistance τ along the melt layer can be expressed by the suspension viscosity η_s and the shear strain rate $d\gamma/dt$, as follows:

$$\tau = \eta_s \cdot (d\gamma/dt). \quad (7)$$

Considering τ along the 1-mm-thick melt layer at a slip rate of 1 m/s and η_s at 1100 °C, τ is in the range of 0.1–0.3 MPa (Table 4). These results indicate the generation of a low-viscosity/low-shear-resistance melt layer during seismic slip, which would induce a dynamic weakness in the fault and cause an increase in the slip rate.

Assuming that most of the mechanical work during faulting is converted to heat and that the shear resistance τ_f of the frictional melt remained constant during slip, τ_f is (Di Toro et al., 2005 and reference therein):

$$\tau_f = \rho\left[C_p(T_m - T_a) + (1-\phi)H\right]w/d \quad (8)$$

where ρ is the rock density, C_p is the specific heat at constant pressure, T_m is the melting temperature, T_a is the ambient temperature, ϕ is the volume fraction of the solid grains, H is the latent heat of fusion, w is the thickness of the friction-induced melt layer, and d is the fault displacement. At present, it is not possible to estimate d because there are no visible offset markers across the pseudotachylytes. Frictional melting occurred at slip rates well in excess of 0.1 m/s (e.g., Sibson, 1975).

Table 4
Suspension viscosities η_s at 1100 °C and corresponding shear resistance τ along 1-mm-thick melt layers at a slip rate of 1 m/s

	Mg-1	Mg-2	Mg-3	Mg-4	Ok-1	Ok-2	Ok-3
η_s (Pa s)	1.9×10^2	1.1×10^2	1.5×10^2	85	1.3×10^2	2.9×10^2	97
τ (MPa)	0.2	0.1	0.2	0.1	0.1	0.3	0.1

Mg: sample from the Mugi area. Ok: sample from the Okitsu area.

Hence, if the slip duration is longer than 1 s, d would be larger than 0.1 m. Given $\rho = 2500\ \mathrm{kg/m^3}$, $C_p = 1000\ \mathrm{J\,kg^{-1}\,^\circ C^{-1}}$, $T_m = 1100\ ^\circ\mathrm{C}$, T_a is 180 °C for the Mugi area and 250 °C for the Okitsu area, ϕ is the data in Table 3, $H = 3.2 \times 10^5\ \mathrm{J\,kg^{-1}}$, $w = 1$ mm, and d ranges from 0.1 to 4 m that corresponds to the fault displacement during earthquakes of magnitudes between $M5$ and $M8$ (Sibson, 1989), then τ_f ranges from 0.7 to 30.3 MPa (Table 5). The shear resistance τ along the pseudotachylyte layer calculated from Eq. (7) (Table 4) is consistent with τ_f during an $M8$ earthquake; this is expected in subduction zones such as the Nankai accretionary margin (Ando, 1975).

The very short cooling time of the frictional melts (Fig. 9) and the microstructures under the BSE and TEM images (Figs. 6 and 7) strongly suggest a rapid solidification of the melt layer. This would result in the rapid healing of the coseismic slip zone (Di Toro and Pennacchioni, 2005). The rapid recovery of fault strength as a result of the rapid healing of the fault subsequent to melt solidification may contribute to the short recurrence time of earthquakes in subduction zones (Kanamori and Heaton, 2000).

The dynamics of frictional melting recorded in the pseudotachylytes of the Shimanto accretionary complex may be applicable to subduction thrusts and faults in other accretionary complexes because illite has been observed elsewhere to be the dominant material in subducted material and sedimentary rocks of exhumed accretionary complexes deformed above 150 °C (e.g., Sample and Moore, 1987; Steurer and Underwood, 2003). Most of the adsorbed and interlayer water of the illite was driven off rapidly below 110 °C, while the remainder was eliminated more slowly between 110 and 350 °C (Deer et al., 1992). Structural water from the $(OH)^-$ ions in the illite was driven off rapidly between 350 and 600 °C. Therefore, illite in the temperature range of a seismogenic subduction zone can preserve chemically bound $(OH)^-$ with little adsorbed and interlayer water. Hence, the melting of the illite-rich slip zone is likely to form a low-viscosity, hydrous melt layer caused by the release of H_2O from the illite.

Laboratory experiments indicate that illite-rich gouge exhibits velocity-strengthening behavior at slip rates of 0.1–200 μm/s (Saffer and Marone, 2003) or stick-slip behavior at slip rates of 0.048 and 4.8 μm/s (Moore et al., 1989). However, there is no experimental data for illite at slip rate higher than 0.1 m/s (seismic slip rates). The illite-rich faults might not nucleate earthquakes, but once earthquake rupture propagates and seismic slip rates are achieved, melt lubrication might be activated, at least locally, with consequent large dynamic stress drop.

Table 5
The shear resistance τ_f of the frictional melt at the given fault displacements d for earthquake magnitudes ranging from $M5$ to $M8$

Magnitude, M		Mg-1	Mg-2	Mg-3	Mg-4	Ok-1	Ok-2	Ok-3
5	d (m)	0.1	0.1	0.1	0.1	0.1	0.1	0.1
	τ_f (MPa)	30.3	28.9	28.9	28.9	28.2	27.8	28.3
6	d (m)	0.4	0.4	0.4	0.4	0.4	0.4	0.4
	τ_f (MPa)	7.6	7.2	7.2	7.2	7.1	7.0	7.1
7	d (m)	1	1	1	1	1	1	1
	τ_f (MPa)	3.0	2.9	2.9	2.9	2.8	2.8	2.8
8	d (m)	4	4	4	4	4	4	4
	τ_f (MPa)	0.8	0.7	0.7	0.7	0.7	0.7	0.7

Mg: sample from the Mugi area. Ok: sample from the Okitsu area.

9. Conclusions

The following conclusions were derived from the analysis of pseudotachylytes in the Shimanto accretionary complex of eastern and western Shikoku, southwest Japan.

1. At seismogenic depths in the subduction zone, a cataclastic thrust zone develops at the top of the mélange, and the coseismic slip is concentrated into a narrow zone less than a few millimeters thick.
2. The pseudotachylyte displays a fragment-laden, glass-supported texture resulting from rapid cooling of the frictional melt, which is consistent with a very short cooling time of the melt layer calculated using thermal modeling. The rapid cooling of the melt layer is due to its narrow thickness, resulting in the fast healing of the coseismic slip zone by the solidified melt layer.
3. The pseudotachylyte is derived from the frictional melting of an illite-rich ultracataclasite layer. The variation in the volume fraction of unmelted grains in the pseudotachylyte matrix primarily represents the difference in the initial volume fraction of illite in the ultracataclasite layer prior to frictional melting. The minimum melting temperature is 1100 °C, which is ~850–920 °C greater than the maximum temperatures recorded in the host rocks.
4. The viscosity and shear resistance of the melt layer are very low; therefore, the dynamic weakness of the fault, acceleration of seismic slip, and propagation of instability can possibly occur during an earthquake. This would contribute, at least locally, to the efficiency with which stored strain energy is released and hence to the earthquake magnitude in subduction zones.
5. Such frictional melting of the illite-rich slip zone may be applicable to subduction thrusts and faults in other accretionary complexes. The melting of the illite-rich slip zone is likely to form a hydrous melt layer, possibly leading to a high H_2O content in these pseudotachylytes.

Acknowledgements

The manuscript benefited from discussions and suggestions by Kenshiro Otsuki, Kieran O'Hara, J. Casey Moore, Anne-Marie Boullier, Masanori Kameyama, Gaku Kimura, and Hisao Ito. The JSG reviewers Giulio Di Toro and John P. Craddock made many valuable comments to improve this manuscript. We thank Alex Maltman for a final reading of the revised manuscript. This research was funded by a Grant-in-Aid for Science Research (B) of the Ministry of Education, Culture, Sports, Science and Technology (project number 17340152).

References

Ando, M., 1975. Source mechanisms and tectonic significance of historical earthquakes along the Nankai Trough, Japan. Tectonophysics 27, 119–140.

Bottinga, T., Weill, D.F., 1972. The viscosity of magmatic liquids: a model for calculations. American Journal of Science 272, 438–475.

Boullier, A.M., Ohtani, T., Fujimoto, K., Ito, H., Dubois, M., 2001. Fluid inclusions in pseudotachylytes from the Nojima fault, Japan. Journal of Geophysical Research 106, 21965–21977.

Carslaw, H.S., Jaeger, J.C., 1959. Conduction of Heat in Solids, second ed. Oxford University Press, New York.

Deer, W.A., Howie, R.A., Zussman, J., 1992. An Introduction to the Rock-forming Minerals, second ed. Green and Co. Ltd., London, Longmans.

Di Toro, G., Pennacchioni, G., 2005. Fault plane processes and mesoscopic structure of a strong-type seismogenic fault in tonalites (Adamello batholith, Southern Alps). Tectonophysics 402, 54–79.

Di Toro, G., Pennacchioni, G., Teza, G., 2005. Can pseudotachylytes be used to infer earthquake source parameters? An example of limitations in the study of exhumed faults. Tectonophysics 402, 3–20.

Di Toro, G., Hirose, T., Nielsen, S., Pennacchioni, G., Shimamoto, T., 2006. Natural and experimental evidence of melt lubrication of faults during earthquakes. Science 311, 647–649.

Fisher, D., Byrne, T., 1987. Structural evolution of underthrusted sediments, Kodiak Island, Alaska. Tectonics 6, 775–793.

Henley, R.W., Ellis, A.J., 1983. Geothermal systems, ancient and modern: a geochemical review. Earth-Science Reviews 19, 1–50.

Hyndman, R.D., Yamano, M., Oleskevich, D.A., 1997. The seismogenic zone of subduction thrust faults. The lsland Arc 6, 244–260.

Ikesawa, E., Sakaguchi, A., Kimura, G., 2003. Pseudotachylyte from an ancient accretionary complex: evidence for melt generation during seismic slip along master décollement? Geology 31, 637–640.

Kanamori, H., Heaton, T.H., 2000. Microscopic and macroscopic physics of earthquakes. In: Rundle, J., Turcotte, D.L., Klein, W. (Eds.), Geocomplexity and the Physics of Earthquakes. Geophysical Monograph, vol. 120, pp. 147–163.

Kennedy, G.C., Wasserburg, G.J., Heard, H.C., Newton, R.C., 1962. The upper three phase region in the system SiO_2–H_2O. American Journal of Science 260, 501–521.

Kitamura, Y., Sato, K., Ikesawa, E., Ohmori, K., Kimura, G., Kondo, H., Ujiie, K., Onishi, C.T., Kawabata, K., Hashimoto, Y., Mukoyoshi, H., Masago, H., 2005. Mélange and its seismogenic roof décollement: a plate boundary fault rock in the subduction zone – an example from the Shimanto Belt, Japan. Tectonics 24, TC5012, doi:10.1029/2004TC001635.

Kitano, T., Kataoka, T., Shirota, T., 1981. An empirical equation of the relative viscosity of polymer melts filled with various inorganic fillers. Rheologica Acta 20, 207–209.

Kraynik, A.M., 1988. Foam flows. Annual Review of Fluid Mechanics 20, 325–357.

Lee, D.I., 1969. The viscosity of concentrated suspensions. Transactions of the Society of Rheology 13, 273–288.

Magloughlin, J.F., 1992. Microstructural and chemical changes associated with cataclasis and frictional melting as shallow crustal levels: the cataclasite–pseudotachylyte connection. Tectonophysics 204, 243–260.

Magloughlin, J.F., Spray, J.G., 1992. Frictional melting processes and products in geological materials: introduction and discussion. Tectonophysics 204, 197–206.

Marone, C., Scholz, C.H., 1988. The depth of seismic faulting and the upper transition from stable to unstable slip regimes. Geophysical Research Letter 15, 621–624.

Metzner, A.B., 1985. Rheology of suspensions in polymeric liquids. Journal of Rheology 29, 739–775.

Moecher, D.P., Brearley, A.J., 2004. Mineralogy and petrology of a mullite-bearing pseudotachylyte: constraints on the temperature of coseismic frictional fusion. American Mineralogist 89, 1486–1495.

Moore, D.E., Summers, R., Byerlee, J.D., 1989. Sliding behavior and deformation textures of heated illite gouge. Journal of Structural Geology 11, 329–342.

Moore, J.C., 1989. Tectonics and hydrogeology of accretionary prisms: role of the décollement zone. Journal of Structural Geology 11, 95–106.

Moore, J.C., Saffer, D., 2001. Updip limit of the seismogenic zone beneath the accretionary prism of southwest Japan: an effect of diagenetic to low-grade metamorphic processes and increasing effective stress. Geology 29, 183–186.

Ohmori, K., Taira, A., Tokuyama, H., Sakaguchi, A., Okamura, M., Aihara, A., 1997. Paleothermal structure of the Shimanto accretionary prism, Shikoku, Japan: role of an out-of-sequence thrust. Geology 25, 327–330.

Oleskevich, D.A., Hyndman, R.D., Wang, K., 1999. The updip and downdip limits to great subduction earthquakes: thermal and structural models of Cascadia, south Alaska, SW Japan, and Chile. Journal of Geophysical Research 104, 14965–14991.

Onishi, C.T., Kimura, G., 1995. Change in fabric of mélange in the Shimanto Belt, Japan: change in relative convergence? Tectonics 14, 1273–1289.

Otsuki, K., Monzawa, N., Nagase, T., 2003. Fluidization and melting of fault gouge during seismic slip: identification in the Nojima fault zone and implications for focal earthquake mechanisms. Journal of Geophysical Research 108, 2192, doi:10.1029/2001JB001711.

Otsuki, K., Uduki, T., Monzawa, N., Tanaka, H., 2005. Clayey injection veins and pseudotachylyte from two boreholes penetrating the Chelungpu Fault, Taiwan: their implications for the contrastive seismic slip behaviors during the 1999 Chi–Chi earthquake. The Island Arc 14, 22–36.

Rowe, C.D., Moore, J.C., Meneghini, F., McKiernan, A.W., 2005. Large-scale pseudotachylytes and fluidized cataclasites from an ancient subduction thrust fault. Geology 33, 937–940.

Saffer, D.M., Marone, C., 2003. Comparison of smectite- and illite-rich gouge frictional properties: application to the updip limit of the seismogenic zone along subduction megathrusts. Earth and Planetary Science Letters 215, 219–235.

Sakaguchi, A., 1996. High paleo-geothermal gradient with ridge subduction beneath Cretaceous Shimanto accretionary prism, southwest Japan. Geology 24, 795–798.

Sample, J.C., Moore, J.C., 1987. Structural style and kinematics of an underplated slate belt, Kodiak and adjacent islands, Alaska. Geological Society of America Bulletin 99, 7–20.

Scholz, C.H., 1980. Shear heating and the state of stress on faults. Journal of Geophysical Research 85, 6174–6184.

Scholz, C.H., 2002. The Mechanics of Earthquakes and Faulting, second ed. Cambridge University Press, New York.

Shaw, H.R., 1972. Viscosities of magmatic silicate liquids: an empirical method of prediction. American Journal of Science 272, 870–893.

Shimozuru, D., 1978. Dynamics of magma in a volcanic conduit: special emphasis on viscosity of magma with bubbles. Journal of Volcanology 41, 333–340.

Shirozu, H., 1988. Introduction to Clay Mineralogy: Fundamentals for Clay Science. Asakura Printing Co. Ltd., Tokyo.

Sibson, R.H., 1975. Generation of pseudotachylyte by ancient seismic faulting. Geophysical Journal of the Royal Astronomical Society 43, 775–794.

Sibson, R.H., 1989. Earthquake faulting as a structural process. Journal of Structural Geology 11, 1–14.

Spray, J.G., 1992. A physical basis for the frictional melting of some rock-forming minerals. Tectonophysics 204, 205–221.

Spray, J.G., 1993. Viscosity determinations of some frictionally generated silicate melts: implications for fault zone rheology at high strain rates. Journal of Geophysical Research 98, 8053–8068.

Spray, J.G., 1995. Pseudotachylyte controversy: fact or friction? Geology 23, 1119–1122.

Steurer, J.F., Underwood, M.B., 2003. Clay mineralogy of mudstones from the Nankai Trough reference Sites 1173 and 1177 and frontal accretionary prism Site 1174. In: Proceedings of ODP Scientific Results [online], 190/196. Available from: http://www-odp.tamu.edu/publications/190196SR/211/211.htm.

Taira, A., Katto, J., Tashiro, M., Okamura, M., Kodama, K., 1988. The Shimanto Belt in Shikoku Japan: evolution of Cretaceous to Miocene accretionary prism. Modern Geology 12, 5–46.

Taylor, G.I., 1932. The viscosity of fluid containing small drops of another fluid. Proceedings of the Royal Society of London A138, 41–48.

Thomas, M.A., 1922. On certain xenoliths in tertiary minor intrusions in the Island of Mull (Argyllshire). Quarterly Journal of the Geological Society of London 78, 229–260.

Turcotte, D.L., Schubert, G., 2002. Geodynamics, second ed. Cambridge University Press, New York.

Uhira, K., 1980. Experimental study on the effect of bubble concentration on the effective viscosity of liquids. Bulletin of the Earthquake Research Institute 55, 857–871.

Ujiie, K., 2002. Evolution and kinematics of an ancient décollement zone, mélange in the Shimanto accretionary complex of Okinawa Island, Ryukyu Arc. Journal of Structural Geology 24, 937–952.

Ujiie, K., Hisamitsu, T., Taira, A., 2003. Deformation and fluid pressure variation during initiation and evolution of the plate boundary décollement zone in the Nankai accretionary prism. Journal of Geophysical Research 108 (B8), 2398, doi:10.1029/2002JB002314.

Underwood, M.B., Hibbard, J.P., DiTullio, L., 1993. Geological summary and conceptual framework for the study of thermal maturity within the Eocene–Miocene Shimanto Belt, Shikoku, Japan. In: Underwood, M.B. (Ed.), Thermal Evolution of the Tertiary Shimanto Belt, Southwest Japan: An Example of Ridge–Trench Interaction. Special Paper Geological Society of America, vol. 273, pp. 1–24.

Vrolijk, P., Myers, G., Moore, J.C., 1988. Warm fluid migration along tectonic mélanges in the Kodiak accretionary complex, Alaska. Journal of Geophysical Research 93, 10313–10324.